Atmospheric Environment 100 (2015) 167–177

Contents lists available at ScienceDirect

Atmospheric Environment

journal homepage: www.elsevier.com/locate/atmosenv

Urban air quality simulation in a high-rise building area using a CFD model coupled with mesoscale meteorological and chemistry-transport models

Kyung-Hwan Kwak [a], Jong-Jin Baik [a, *], Young-Hee Ryu [a, b], Sang-Hyun Lee [c]

[a] School of Earth and Environmental Sciences, Seoul National University, Seoul 151-742, Republic of Korea
[b] Department of Civil and Environmental Engineering, Princeton University, NJ 08544, USA
[c] Department of Atmospheric Science, Kongju National University, Gongju 314-701, Republic of Korea

HIGHLIGHTS

- An integrated urban air quality modeling system is developed based on a CFD model.
- The WRF and CMAQ models provide time-dependent boundary conditions of the CFD model.
- Simulation results show good agreements with the measurement at an on-road site.
- NO_2 and O_3 dispersion in a high-rise building area is realistically simulated.
- Spatial variability of air quality is associated with buildings and mobile emission.

ARTICLE INFO

Article history:
Received 13 August 2014
Received in revised form
28 October 2014
Accepted 30 October 2014
Available online 1 November 2014

Keywords:
Urban air quality
Integrated urban air quality modeling system
CFD model
WRF model
CMAQ model
High-rise building area

ABSTRACT

An integrated urban air quality modeling system is established by coupling a computational fluid dynamics (CFD) model with mesoscale meteorological and chemistry-transport models. The mesoscale models used are the weather research and forecasting (WRF) model and the community multiscale air quality (CMAQ) model, which provide the initial and time-dependent boundary conditions for the CFD model. For the consistency of chemical processes in the CFD and CMAQ models, the same chemical mechanism used in the CMAQ model is implemented in the CFD model. Urban air quality simulations are performed from 0900 to 1800 LT on 3 June 2010 in a high-rise building area of Seoul, Republic of Korea, where mobile emission sources are concentrated. The NO_2 and O_3 concentrations in the CFD simulation are evaluated with data measured at a roadside air quality monitoring station, showing better agreements than those in the CMAQ simulation. The NO_2 and O_3 concentration fields exhibit high spatial variabilities in the high-rise building area. The spatial variabilities near the surfaces are strongly associated with the heterogeneity of mobile emission on roads, whereas the spatial variabilities near the top of high-rise buildings are strongly associated with the heterogeneity of building geometry. The average NO_2 and O_3 concentrations (46 and 30 ppb, respectively, at $z = 30$ m) near the surfaces are considerably different from the NO_2 and O_3 concentrations in the CMAQ simulation (17 and 44 ppb, respectively, at $z = 30$ m), implying the insufficient urban surface representation in the CMAQ simulation. The heterogeneity of building geometry is found to enhance the vertical pollutant transport, whereas the heterogeneity of mobile emission is found to confine emitted pollutants near the surfaces. When the vertical mixing is efficient, the O_3 concentration decreases in substantial vertical ranges with the same amount of NO_x emission. The integrated urban air quality modeling system realistically simulates the spatial variabilities associated with the local influences of building geometry and mobile emission. This is a promising modeling approach that accounts for multiscale influences on urban air quality.

* Corresponding author.
E-mail address: jjbaik@snu.ac.kr (J.-J. Baik).

http://dx.doi.org/10.1016/j.atmosenv.2014.10.059
1352-2310/

1. Introduction

Urban air quality, which is typically represented by several key pollutant concentrations, generally exhibits a significant variability. The high spatial variability of air quality in an urban area is mainly attributed to local emission sources, whereas the high seasonal variability of air quality is mainly attributed to regional emission sources (Clapp and Jenkin, 2001; Jenkin, 2004). Particularly in densely built-up areas where many residents, drivers, and walkers are concentrated, on-road mobile emission is one of the main contributors to the spatial variability of air quality (Vardoulakis et al., 2011). Many field measurement studies (Kaur et al., 2005; Anttila et al., 2011; Shon et al., 2011; Mavroidis and Ilia, 2012) have consistently reported that considerably higher concentrations of primary pollutants (e.g., NO_x, CO, and particulate matter (PM)) are measured near roads compared with the urban background. Matte et al. (2013) investigated the intraurban spatial patterns of multiple air pollutants and reported that not only primary pollutants but also secondary pollutants exhibit substantial spatial variabilities at street-level sites.

Extensive and simultaneous monitoring of many pollutant concentrations in a small urban area, however, has practical constraints such as a high cost and the low availability of space. In comparison, numerical simulations can flexibly assess air quality in a small urban area with a diverse range of experimental settings. Building-scale air quality has recently been investigated using computational fluid dynamics (CFD) models that explicitly resolve buildings and roads. Several comparison studies using CFD models coupled with simple $NO–NO_2–O_3$ chemistry and more complex chemistry have shown that a detailed description of volatile organic compounds (VOC) chemistry is required to accurately simulate reactive pollutant concentrations even in small urban areas (Wang et al., 2011; Karim and Nolan, 2011; Kim et al., 2012; Bright et al., 2013). The spatial variations of reactive pollutant dispersion significantly depend on local factors such as the NO_x-to-VOC ratio of mobile emission (Kwak and Baik, 2012), canyon aspect ratio (Kwak et al., 2013), and surface heating (Kwak and Baik, 2014).

Local-scale dispersion models have been coupled with mesoscale models to consider larger-scale influences appropriately in a single modeling framework (Stein et al., 2007; Isakov et al., 2009; Beevers et al., 2012). Beevers et al. (2012) coupled the community multiscale air quality (CMAQ) modeling system and a Gaussian-type plume model with simple $NO–NO_2–O_3$ chemistry and simulated hourly, monthly, and annual NO_2 and O_3 concentrations in London. With advances in the coupling method of a CFD model, a mesoscale meteorological model can provides time-dependent boundary conditions of a CFD model for meteorological variables (e.g., Chen et al., 2011). Scalar dispersion in built-up areas has been simulated using CFD models with time-dependent boundary conditions provided by mesoscale meteorological models for point emission sources by Baik et al. (2009), Tewari et al. (2010), Wyszogrodzki et al. (2012), and Michioka et al. (2013) and for on-road emission by Liu et al. (2012). In contrast to the simulations of scalar dispersion assuming zero background concentration, a simulation of reactive pollutant dispersion in an urban area using a coupled CFD model remains a challenge because of the need for time-dependent boundary conditions for various pollutants. The coupling method of a CFD model that incorporates a chemical mechanism with a mesoscale chemistry-transport model is essential to solve this challenging problem. The first aim of this study is to develop an integrated urban air quality modeling system by coupling a CFD model with both mesoscale meteorological and chemistry-transport models, which is a first attempt.

The intraurban spatial variability of air quality has not typically been considered in numerical studies that use mesoscale chemistry-transport models. Using the integrated urban air quality modeling system, a part of urban area (i.e., a few km^2 in size) that has usually been considered in a grid cell of a chemistry-transport model domain can be fully resolved at a building and road scale. Then, it is feasible to numerically examine the intraurban spatial variability of air quality associated with building geometry and mobile emission. This is a straight-forward way to remove uncertainties when simulating pollutant concentrations assuming instantaneous well-mixing within a grid cell of the chemistry-transport model domain (Auger and Legras, 2007). The second aim of this study is to compare the results of the integrated urban air quality modeling system with the corresponding results of chemistry-transport model and discuss how the spatial variabilities associated with urban surface characteristics are projected in representative air quality.

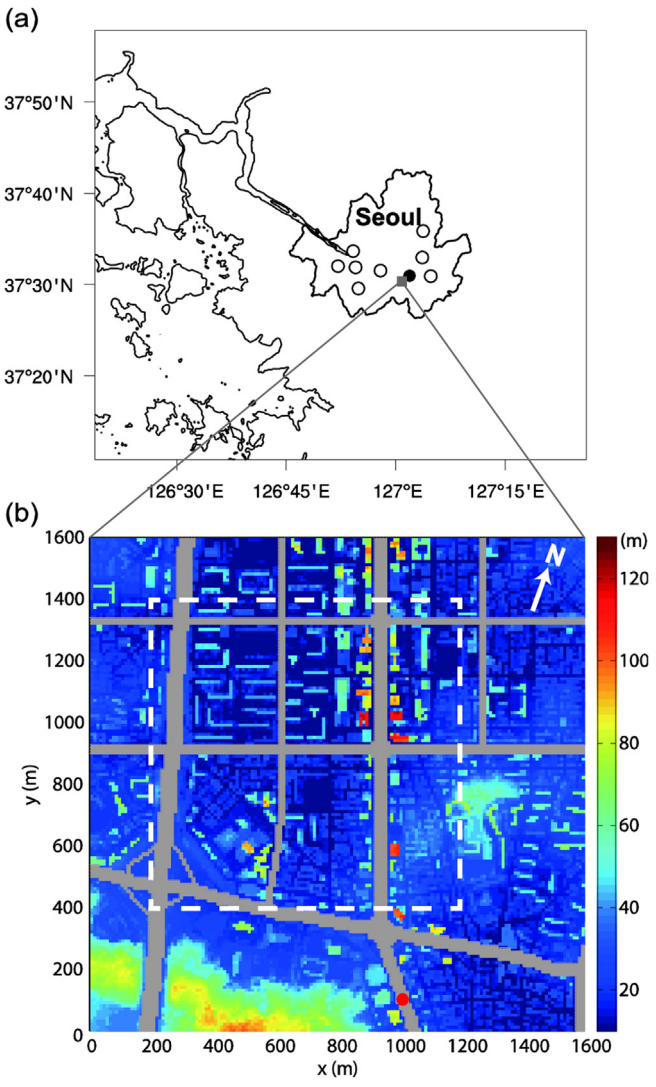

Fig. 1. (a) The innermost mesoscale model domain and (b) the surface heights in the CFD model domain. In (a), open circles indicate the locations of automatic weather stations (AWSs) in Seoul, and a closed circle indicates the location of Gangnam AWS. In (b), a boxed area with a white dashed line is considered for analysis of CFD simulation results, and a red circle indicates the location of roadside air quality monitoring station.

2. Multiscale modeling framework

2.1. Coupling methodology

A CFD model that is a Reynolds-averaged Navier–Stokes equations (RANS) model with the renormalization group (RNG) k–ε turbulence closure scheme (Kim and Baik, 2004; Baik et al., 2007) is coupled with the weather research and forecasting (WRF) model version 3.2 (Skamarock et al., 2008) and the CMAQ model version 4.7.1 (Byun and Schere, 2006). For the consistency of chemical processes in the CFD and CMAQ models, the statewide air pollution research center version 99 (SAPRC-99) chemical mechanism (Carter, 2000) and the Eulerian backward iteration (EBI) method (Hertel et al., 1993) used in the CMAQ model are implemented in the CFD model.

One-way coupling is employed. The vertical profiles of horizontal wind components, air temperature, and turbulent kinetic energy and the 2-m air temperature obtained from the WRF simulation and the pollutant concentration profiles, mobile emission rates, and photolysis rates obtained from the CMAQ simulation are used as the initial and/or boundary conditions in the CFD simulation. The horizontal wind components, air temperature, turbulent kinetic energy, 2-m air temperature, and pollutant concentrations are collected every 30 min, and the mobile emission and photolysis rates are collected every 60 min. The horizontal wind components, air temperature, turbulent kinetic energy, and pollutant concentrations obtained from the vertical levels of the mesoscale model domains are linearly interpolated at every vertical level of the CFD model domain. The 2-m air temperature obtained from the WRF simulation is used to specify the air temperature at the grid points closest to the horizontal surfaces in the CFD simulation, while the adiabatic boundary condition is adopted at the grid points closest to the vertical surfaces (e.g., building walls). The mobile emission rates are spatially allocated on roads in the CFD model domain. The photolysis rates are uniformly adopted in the CFD model domain. To update the time-dependent input data in the CFD simulation, the linear interpolation in time is applied at every dynamics time step for the data obtained from the mesoscale simulations.

2.2. Mesoscale simulations

The WRF and CMAQ simulations are performed for the period from 2100 LT (=UTC + 9 h) on 1 June 2010 to 0900 LT on 4 June 2010. In the WRF simulation, four nested domains with horizontal grid sizes of 27, 9, 3, and 1 km are adopted. Seoul (37°N, 127°E), a megacity in Republic of Korea, is located in the middle of the innermost mesoscale model domain (Fig. 1a). The Mellor–Yamada–Janjić (MYJ) planetary boundary layer (PBL) scheme (Mellor and Yamada, 1982; Janjić, 1994) that prognostically calculates turbulent kinetic energy and the Seoul National University urban canopy model (SNUUCM; Ryu et al., 2011) are used. This study takes account of the gridded anthropogenic heat data established by Lee et al. (2009).

In the CMAQ simulation, three nested domains with horizontal grid sizes of 9, 3, and 1 km are adopted. The SAPRC-99 chemical mechanism and the fifth-generation CMAQ aerosol module (AERO5) (Foley et al., 2010) are used. The anthropogenic pollutant emissions are prepared using the sparse matrix operator kernel emissions (SMOKE) system (Houyoux et al., 2000). The 2007 clean air policy support system (CAPSS) (Moon et al., 2006) data updated by Ryu et al. (2013) for year of 2008 are used as the anthropogenic emission inventory in Republic of Korea. The biogenic pollutant emissions are prepared using the model of emissions of gases and aerosols from nature (MEGAN) (Guenther et al., 2006). The CMAQ default concentration profiles are applied at the boundaries of outermost domain.

2.3. CFD simulation

A CFD simulation is performed for the period from 0900 to 1800 LT on 3 June 2010 in a high-rise building area of Seoul. The domain size is 1600 m in the x- and y-directions and 997 m in the z-

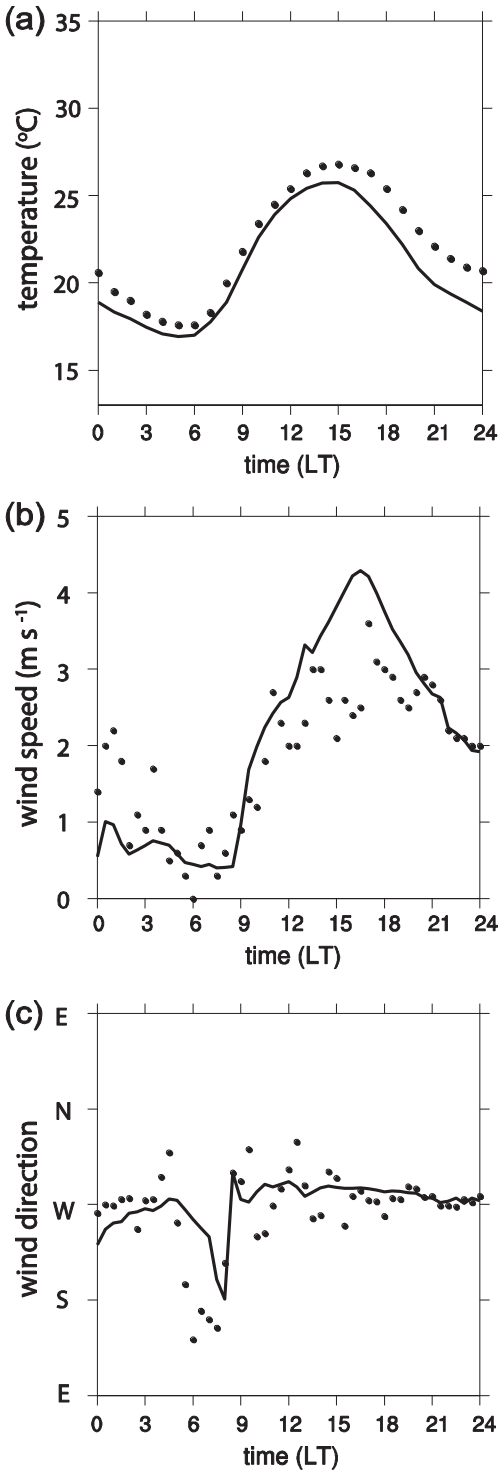

Fig. 2. (a) Diurnal variations of the simulated (line) and measured (dot) near-surface air temperatures averaged over 9 AWSs in urban areas of Seoul on 3 June 2010. The diurnal variations of the simulated (line) and measured (dot) near-surface (b) wind speeds and (c) directions at Gangnam AWS (AWS closest to the study area for the CFD simulation) on 3 June 2010.

direction (corresponding to the vertical range up to the 11th vertical model level in the mesoscale simulations). The number of grids is 160 × 160 × 106. The grid size is 10 m in the *x*- and *y*-directions. The grid size is 4 m in the *z*-direction below $z = 200$ m. In the CFD model domain, the surface heights that include topographical and building heights are estimated using the airborne light detection and ranging (LIDAR) measurement in 2008 (Fig. 1b). The surface heights range from $z = 8$ to 124 m.

The governing equations consisting of the momentum equation, the mass continuity equation, the thermodynamic energy equation, the equations of turbulent kinetic energy and its dissipation rate, and the transport equations of reactive species are integrated. After the first 10-min model run (at 0910 LT), the transport, dry deposition, and emission terms in the transport equations are activated. The chemical production term calculated by the SAPRC-99 chemical mechanism is activated at 0920 LT. The dynamics and chemistry time steps are 1 and 60 s, respectively. The dry deposition term is calculated at all surfaces with constant deposition velocities of, for example, 0.063 cm s^{-1} for NO_2, 0.12 cm s^{-1} for O_3, and 8 cm s^{-1} for HNO_3, following Kwak and Baik (2014). Mobile emission is spatially allocated on roads in the CFD model domain (Fig. 1b). The NO_2-to-NO_x ratio of mobile emission is assigned to 0.2 based on the recent report for Seoul (Shon et al., 2011). The diurnal variation of mobile emission rate is also adjusted based on actual traffic counts at a location close to the study area.

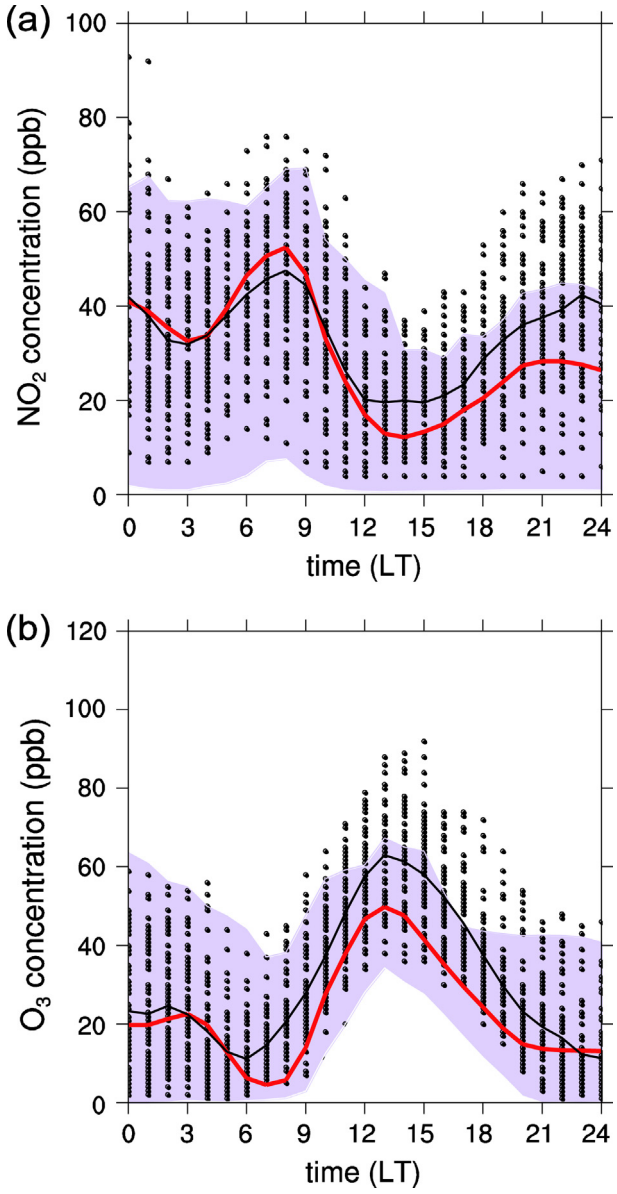

Fig. 3. Diurnal variations of the simulated (red) and measured (black) near-surface (a) NO_2 and (b) O_3 concentrations averaged over 71 air quality monitoring stations in the innermost CMAQ model domain on 3 June 2010. Lines indicate the averaged concentrations, and shaded areas (purple) indicate the ranges of the simulated concentrations over 71 air quality monitoring stations.

3. Evaluation

3.1. WRF simulation

Fig. 2a shows the diurnal variations of the simulated and measured near-surface air temperatures averaged over nine automatic weather stations (AWSs) (circles in Fig. 1a) on 3 June 2010. The cloud cover at Seoul meteorological observatory was 0/10–1/10 on this day under the prevailing high-pressure system. The daily maxima of the simulated and measured average air temperatures are 25.7 and 26.8°C, respectively, at 1500 LT. The underestimated air temperature is to some extent caused by the daytime development of clouds in the WRF simulation. Although the air temperature is slightly underestimated, its diurnal pattern is quite well reproduced in the WRF simulation.

Fig. 2b and c shows the diurnal variations of the simulated and measured near-surface wind speeds and directions at Gangnam AWS (a filled circle in Fig. 1a) on 3 June 2010. The WRF model reproduces the low wind speeds in the early morning and the trend of increasing wind speed until the late afternoon. In addition, the WRF model accurately reproduces the northwesterly to westerly wind during the daytime, especially for the period of CFD simulation, which guarantees the accurate inputs of horizontal wind components at the inflow and outflow boundaries of the CFD model domain.

3.2. CMAQ simulation

Fig. 3 shows the diurnal variations of the simulated and measured near-surface NO_2 and O_3 concentrations averaged over 71 air quality monitoring stations in the innermost CMAQ model domain on 3 June 2010. While the NO_2 concentration ranges widely from a few to tens ppb at a certain time, the daily maxima of the simulated and measured average NO_2 concentrations are 53 and 48 ppb, respectively, at 0800 LT. The average NO_2 concentration is consistently underestimated from 1000 LT. The daily maxima of the simulated and measured average O_3 concentrations are 50 and 63 ppb, respectively, at 1300 LT. The maximum O_3 concentration measured at any air quality monitoring station is 92 ppb at 1500 LT, which is not reproduced in the CMAQ simulation. In general, the average O_3 concentration is consistently underestimated for the period of CFD simulation.

The underestimated average NO_2 and O_3 concentrations for the period of CFD simulation may result from improper boundary conditions for pollutant concentrations in the CMAQ simulation. The prevailing westerly wind on 3 June 2010 could enhance the long-range transport of pollutants such as NO_2 and O_3 emitted or chemically produced in the west (i.e., the Yellow Sea or China). In addition, the urban surface representation may have been insufficient in the CMAQ simulation. Because the simulated NO_2 and O_3 concentrations are evaluated against the measured values near surfaces in urban areas, urban surface characteristics such as building geometry and mobile emission most likely influence the measured NO_2 and O_3 concentrations. This is a shortcoming of

mesoscale chemistry-transport models, which can be resolved by using the integrated urban air quality modeling system.

3.3. CFD simulation

The simulated NO_2 and O_3 concentrations by the integrated urban air quality modeling system are evaluated against the measured values at a roadside air quality monitoring station (a red circle in Fig. 1b) on 3 June 2010 and compared with those by the CMAQ model (Fig. 4). Note that an inlet height of the roadside air quality monitoring station is 4 m above the road surface. As expected from the proximity to the mobile NO_x emission source, the NO_2 concentration is considerably higher in the CFD simulation than in the CMAQ simulation, whereas the O_3 concentration is considerably lower in the CFD simulation than in the CMAQ simulation. It is obvious that the measured NO_2 concentration is better reproduced in the CFD simulation than in the CMAQ simulation. The daily maxima of the simulated and measured O_3 concentrations are 34 (in the CFD simulation) and 33 ppb, respectively. The measured O_3 concentration is close to the simulated value in the CFD simulation until 1400 LT but close to the simulated value in the CMAQ simulation in the late afternoon. The large deviation of O_3 concentration in the CFD simulation in the late afternoon is basically attributed to the underestimated O_3 concentration in the CMAQ simulation as discussed with Fig. 3b. Obviously, the evaluation of CFD simulation for pollutant concentrations would be better to be performed against measured values at multiple monitoring stations in the CFD model domain, which requires an intensive measurement campaign. Particularly for the near-road air quality simulation in the high-rise building area, the integrated urban air quality modeling system generally shows close agreements with the measurement.

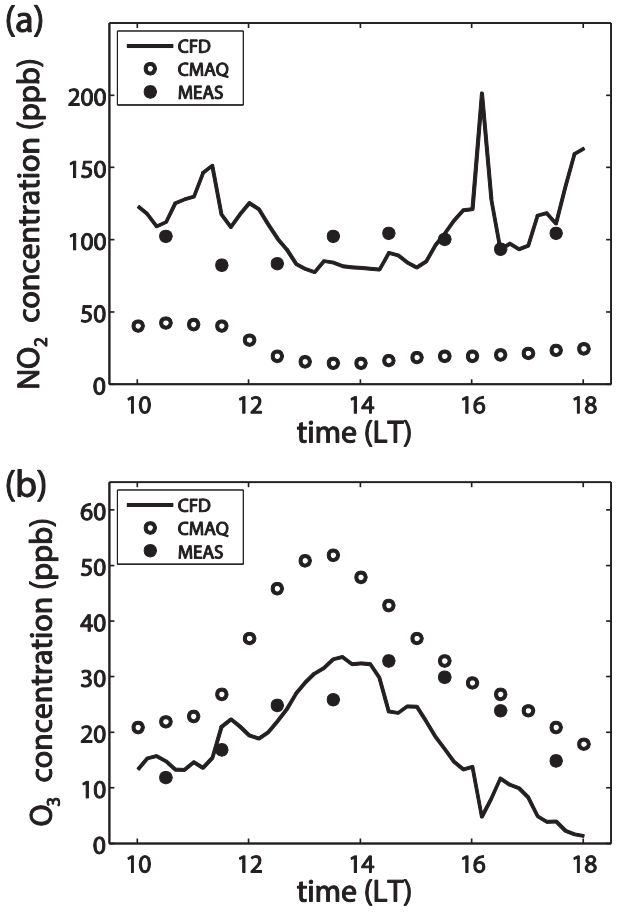

Fig. 4. Temporal variations of the simulated (line, open circle) and measured (closed circle) near-surface (a) NO_2 and (b) O_3 concentrations at a roadside air quality monitoring station indicated by a red circle in Fig. 1b on 3 June 2010.

4. Results and discussion

4.1. Control simulation

The 1 km × 1 km area (a box indicated by a white dashed line in Fig. 1b) is considered for the analysis of CFD simulation. This area includes a highway (x ~ 200 m) and a main road (x ~ 950 m) approximately parallel to each other and many high-rise buildings along the main road. The orientation of the main road in this area is 21° from due north. The 8-h CFD simulation results from 1000 to 1800 LT are analyzed.

Fig. 5 shows the NO_2 and O_3 concentration fields at $z = 30$ m at 1200, 1400, and 1600 LT. Note that the height of $z = 30$ m in the CFD model domain corresponds approximately to the height of the lowest CMAQ model level. The high NO_2 (>100 ppb) and low O_3 (<10 ppb) concentrations are apparent above roads at these times. This is attributed to the freshly-emitted NO_x from vehicles on roads. The polluted air is shown to be minimally dispersed around the roads due to the trapping between buildings. At 1400 LT, for example, an area of an apartment complex (x ~ 650 m, y ~ 1050 m) exhibits relatively low NO_2 and high O_3 concentrations that are more closely approximated to their ambient concentrations. The inverse relationship between the NO_2 and O_3 concentrations results from the NO titration of O_3 that is the most dominant chemical process near mobile NO_x emission sources. Therefore, it is revealed in Fig. 5 that the high NO_2 and O_3 spatial variabilities at this height are strongly associated with the mobile emission on roads.

Fig. 6 shows the NO_2 and O_3 concentration fields at $z = 74$ m at 1200, 1400, and 1600 LT. Note that the height of $z = 74$ m in the CFD model domain corresponds approximately to the height of the second lowest CMAQ model level. Many high-rise buildings along the main road are shown in the concentration fields. The high NO_2 and low O_3 concentrations are apparent around the high-rise buildings. As the ambient wind speed increases over time until 1600 LT (Fig. 2b), elongated plume-like NO_2 dispersion patterns appear downwind of the high-rise buildings, especially at 1400 and 1600 LT. Around the high-rise buildings, the low O_3 concentration remains distinct at this height. At 1400 LT, for example, the O_3 concentration around and downwind of the high-rise buildings is lower than 20 ppb, while the ambient O_3 concentration is higher than 50 ppb. Therefore, it is revealed in Fig. 6 that the high NO_2 and O_3 spatial variabilities at this height are strongly associated with the high-rise buildings.

Fig. 7 shows the NO_2 and O_3 concentrations and streamline fields at $y = 1025$ m at 1200, 1400, and 1600 LT. The width of the main road is 40 m from $x = 930$ to 970 m. At 1200 LT, when the ambient wind is relatively weak, there is little vortex-type flow in street canyons. As the ambient wind speed increases over time, the upward NO_2 transport from the main road to the top of buildings following the apparent clockwise vortex becomes significant, coincident with the low O_3 concentration. This is a well-known phenomenon in a street canyon examined by previous studies (e.g., Baik et al., 2007). The elongated plume-like NO_2 dispersion around the high-rise buildings shown in Fig. 6 is originated from the upward NO_2 transport along building walls.

The area averages of NO_2 and O_3 concentrations over the 1 km × 1 km area in the CFD simulation are systematically compared with the NO_2 and O_3 concentrations in the CMAQ simulation to examine how the spatial variabilities are projected in

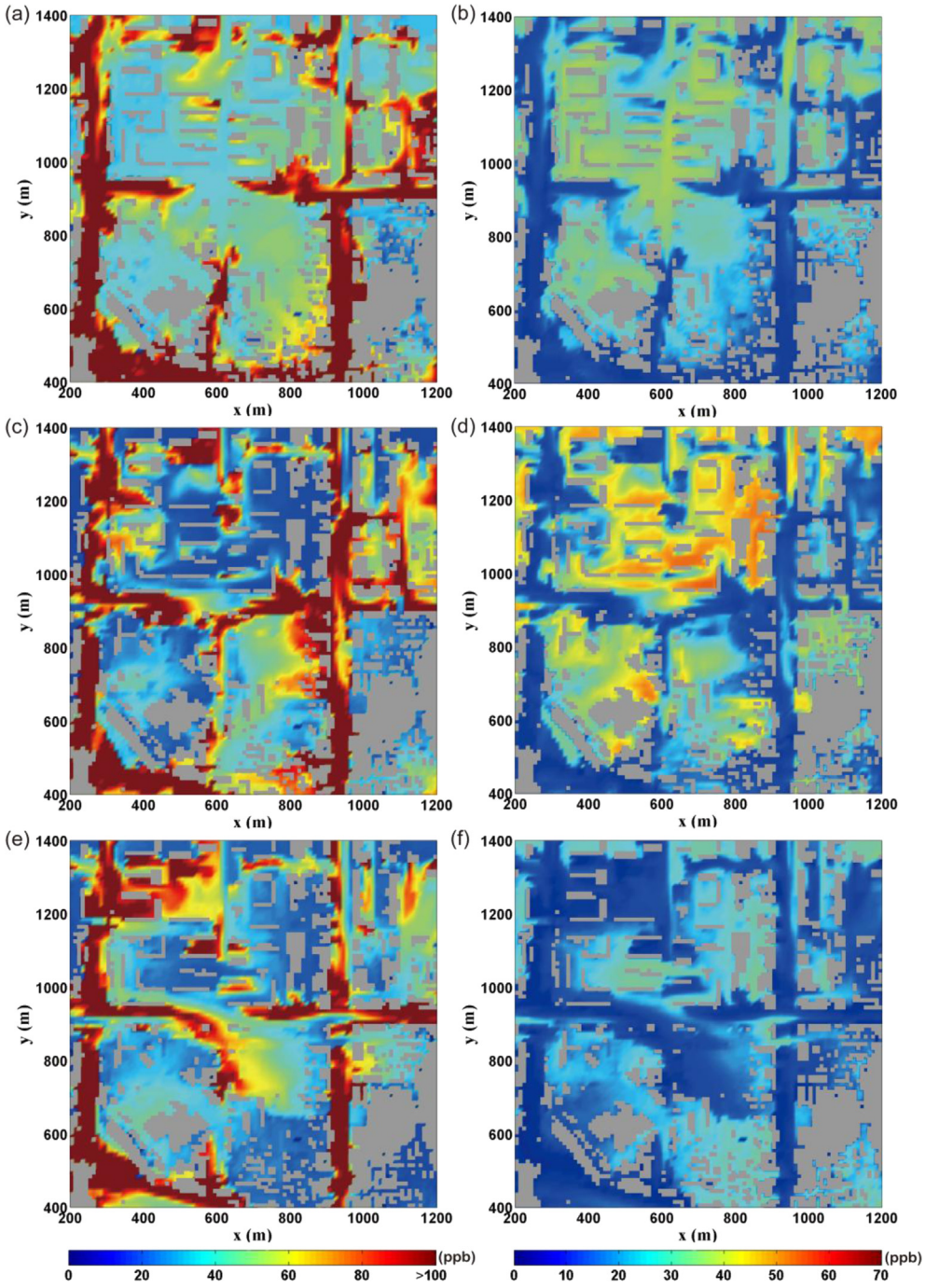

Fig. 5. (left panels) NO_2 and (right panels) O_3 concentration fields at $z = 30$ m at (a, b) 1200, (c, d) 1400, and (e, f) 1600 LT.

the representative air quality. Fig. 8 shows the vertical profiles of the area-averaged NO_2, O_3, and O_x concentrations at 1000, 1200, 1400, and 1600 LT in the CFD simulation. In addition, the vertical profiles of area averages in the CFD simulation and the vertical profiles in the CMAQ simulation are identically averaged for 4 h from 1200 to 1600 LT and are shown in Fig. 8. O_x is simply defined as the sum of NO_2 and O_3, therefore, conserved during the rapid NO_2-to-O_3 conversion. The NO_2 concentration decreases with height and exhibits large vertical gradients near the surfaces. At higher heights (e.g., $z > 100$ m), the NO_2 concentrations until 1200 LT are considerably higher than those in the afternoon. On the other hand, the NO_2 concentration differences between different times are relatively small near the surfaces. While the NO_2 concentration at higher heights is largely related to that in the CMAQ simulation, the NO_2 concentration near the surfaces is more closely related to local influences (e.g., mobile emission, trapping in building canopy, etc.) that are relatively less variable over time. The O_3 concentration increases with height and is the highest at 1400 LT. At each selected time, the vertical gradient of O_3 concentration is larger below $z \sim 40$ m than above $z \sim 40$ m. The 4-h averaged O_3 concentration in the CFD simulation (30 ppb at $z = 30$ m) is considerably lower than that in the CMAQ simulation (44 ppb at $z = 30$ m) below $z \sim 40$ m. In the CFD simulation, the NO titration of O_3 dominantly occurs in limited spaces mostly near roads (Fig. 5). This inefficient O_3

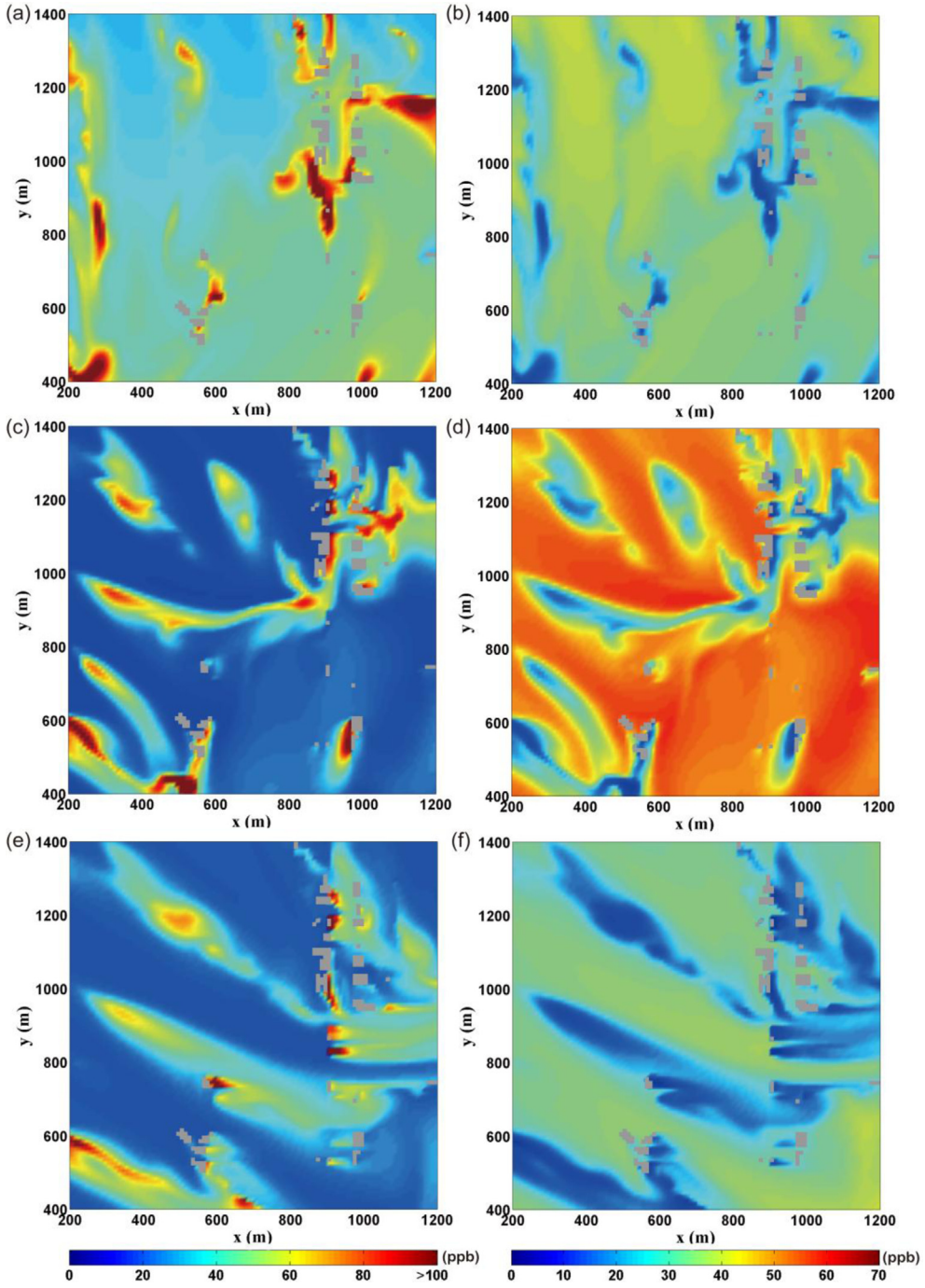

Fig. 6. (left panels) NO_2 and (right panels) O_3 concentration fields at $z = 74$ m at (a, b) 1200, (c, d) 1400, and (e, f) 1600 LT.

titration enables a large amount of NO to be transported to the top of high-rise buildings (Fig. 7). It is interesting that the 4-h averaged O_x concentration in the CMAQ simulation (~61 ppb) is almost vertically uniform. Hence, the increase in 4-h averaged O_x concentration below $z \sim 40$ m in the CFD simulation reflects the local influences of building geometry and mobile emission on the NO_2 and/or O_3 concentrations.

Fig. 9 shows the temporal variations of the area-averaged NO_2 and O_3 concentrations at $z = 30$, 74, and 142 m (the three lowest model levels in the CMAQ simulation). The temporal variations of NO_2 and O_3 concentrations in the CFD simulation generally follow those in the CMAQ simulation. However, the temporal variability at $z = 30$ m is higher in the CMAQ simulation than in the CFD simulation because of the mobile emission that is less variable over time. The differences in NO_2 and O_3 concentrations at different heights are much larger in the CFD simulation than in the CMAQ simulation, implying the better representation of local influences associated with the building geometry and mobile emission in the CFD simulation.

4.2. Comparison simulations

From the discussion above, it is concluded that the heterogeneities of building geometry and mobile emission strongly affect not only the spatial variability of air quality but also the

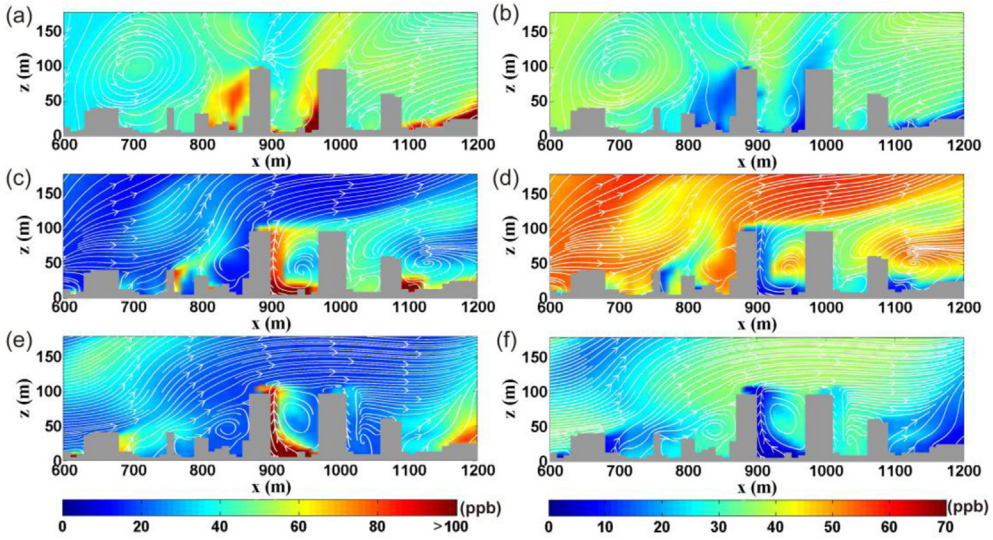

Fig. 7. (left panels) NO_2 and (right panels) O_3 concentrations and streamline fields at $y = 1025$ m at (a, b) 1200, (c, d) 1400, and (e, f) 1600 LT.

representative air quality. To quantify the impacts of heterogeneities, three additional CFD simulations (i.e., ROAD + GRD, LYR + BLD, and LYR + GRD simulations) are performed, which are combinations of two different experimental setups: ROAD/LYR and BLD/GRD. Here, the ROAD + GRD simulation refers to a simulation with the topographical height data removing building height from the surface height data but the same pollutant emission on roads as that in the control CFD simulation (i.e., ROAD + BLD simulation). The LYR + BLD simulation refers to a simulation with the homogeneous pollutant emission distributed in the layer from surfaces to $z = 50$ m but with the same surface height data as that in the control CFD simulation. The LYR + GRD simulation refers to a simulation including both the modified surface height data and the homogeneous pollutant emission. The total pollutant emissions over the 1.6 km × 1.6 km area in the three additional simulations are the same as that in the control CFD simulation.

The vertical profiles of the time- and area-averaged NO_2, O_3, and O_x concentrations in the four different CFD simulations are compared in Fig. 10. Note that the concentrations are averaged over the 1.6 km × 1.6 km area to take the same pollutant emission into account in the analysis. While the NO_2 concentration decreases with height, the decreasing rate of NO_2 concentration with height is smaller near the surfaces in the ROAD + BLD simulation than in the ROAD + GRD simulation. Therefore, the increasing rate of O_3 concentration with height is also smaller near the surfaces in the ROAD + BLD simulation than in the ROAD + GRD simulation. In the presence of buildings, the NO_2 concentration increases by 7.4 ppb (15%) and 4.1 ppb (15%) at $z = 30$ and 74 m, respectively, and the O_3 concentration decreases by 5.9 ppb (21%) and 3.7 ppb (9%) at $z = 30$

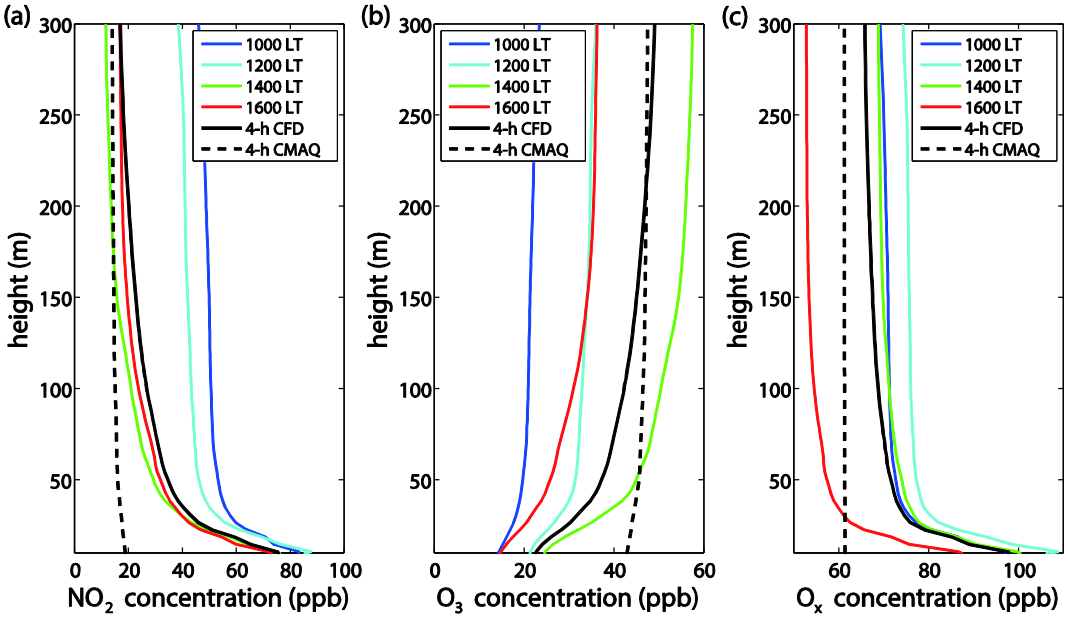

Fig. 8. Vertical profiles of the area-averaged (a) NO_2, (b) O_3, and (c) O_x concentrations at 1000, 1200, 1400, and 1600 LT in the CFD simulation. The vertical profiles of the area averages in the CFD simulation (black solid line) and the vertical profiles in the CMAQ simulation (black dashed line) are averaged for 4 h from 1200 to 1600 LT.

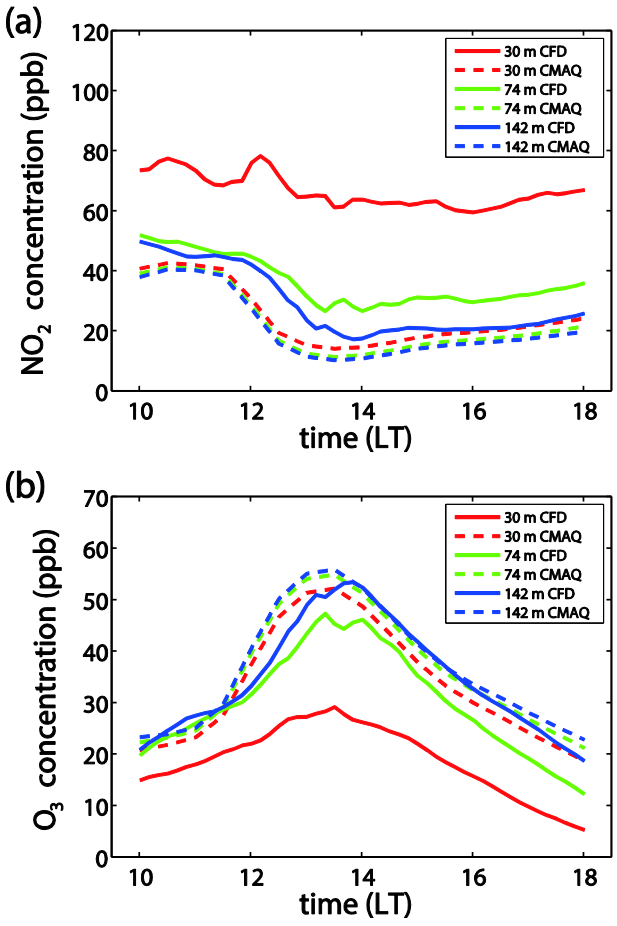

Fig. 9. Temporal variations of the area-averaged (a) NO_2 and (b) O_3 concentrations in the CFD simulation (solid line) and CMAQ simulation (dashed line) at $z = 30$, 74, and 142 m.

and 74 m, respectively. It is noteworthy that the impact of building geometry on the O_x concentration is insignificant because O_x is independent of the NO titration of O_3. The comparison of the vertical concentration profiles between the ROAD + BLD and ROAD + GRD simulations confirms that the heterogeneity of building geometry promotes the vertical transport of NO_x emitted on roads followed by the enhanced NO titration of O_3. The emitted pollutants in the LYR + BLD simulation are artificially well-mixed near the surfaces by its experimental setup. Therefore, the NO_2 concentration in the LYR + BLD simulation is higher by 5.2 ppb (11%) and 1.4 ppb (5%) at $z = 30$ and 74 m, respectively, than that in the ROAD + BLD simulation. As the NO titration of O_3 is efficient, the O_3 concentration in the LYR + BLD simulation is lower by 6.0 ppb (21%) and 1.0 ppb (2%) at $z = 30$ and 74 m, respectively, than that in the ROAD + BLD simulation. The comparison of the vertical concentration profiles between the ROAD + BLD and LYR + BLD simulations confirms that the heterogeneity of mobile emission realistically distributed on roads confines the emitted pollutants near the surfaces, resulting in the weakened NO titration of O_3.

The impacts of high-rise buildings and mobile emission are elaborated by the segregation effects (Auger and Legras, 2007; Zhong et al., 2014). In the previous studies, the segregation effects become significant as the pollutant mixing is less efficient, resulting in the higher O_3 concentration due to the weakened NO titration of O_3. In this study, the impacts of heterogeneities of building geometry and mobile emission on air quality in the high-rise building area are compensated by each other. As an example, the NO_2 and O_3 concentration differences between the ROAD + BLD and LYR + GRD simulations are relatively small, which are 0.5 ppb (1%) and 1.6 ppb (6%), respectively, at $z = 30$ m. In addition, the impacts are less significant above the top of high-rise buildings. The NO_2 and O_3 concentration differences at $z = 142$ m are at most 0.6 ppb (3%) and 0.7 ppb (2%), respectively.

5. Summary and conclusions

Urban air quality simulations were performed using an integrated urban air quality modeling system developed by coupling a CFD model with WRF and CMAQ models. The horizontal wind

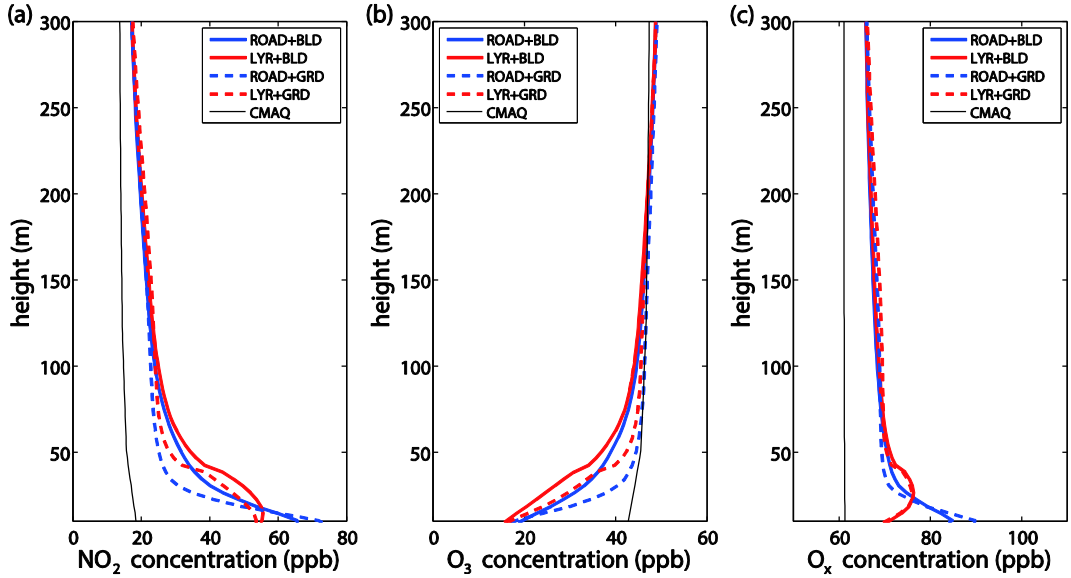

Fig. 10. Vertical profiles of the area- and time-averaged (a) NO_2, (b) O_3, and (c) O_x concentrations in the ROAD + BLD, LYR + BLD, ROAD + GRD, and LYR + GRD simulations. The vertical profiles of the area averages over the 1.6 km × 1.6 km area and the vertical profiles in the CMAQ simulation are averaged for 4 h from 1200 to 1600 LT.

components, air temperature, and turbulent kinetic energy obtained from the WRF simulation and the pollutant concentrations, mobile emission rates, and photolysis rates obtained from the CMAQ simulation were provided as initial and time-dependent boundary conditions of the CFD model. A high-rise building area of Seoul, Republic of Korea, was chosen for the urban air quality simulations on 3 June 2010. The surface height and road distribution data were included in the CFD model domain. The NO_2 and O_3 concentrations in the CMAQ simulation were evaluated against the measurements, showing underestimations for the period of CFD simulation. The NO_2 and O_3 concentrations in the CFD simulation were evaluated with measured data at a roadside air quality monitoring station, showing the better agreements than those in the CMAQ simulation. The NO_2 and O_3 dispersion exhibits the high spatial variabilities associated with the local influences of high-rise buildings and mobile emission. The area averages of NO_2 and O_3 concentrations over the 1 km $\times$ 1 km area in the CFD simulation are largely deviated from the NO_2 and O_3 concentrations, respectively, in the CMAQ simulation especially near the surfaces. The higher NO_2 concentration and lower O_3 concentration in the CFD simulation near the surfaces are attributed to the building geometry and mobile emission. The comparison simulations without building geometry and/or with homogenous pollutant emission in a layer were performed to examine the impacts of local influences on the representative urban air quality. The heterogeneity of building geometry enhances the vertical pollutant transport, while the heterogeneity of mobile emission realistically distributed on roads confines the emitted pollutants near the surfaces. As a result, the O_3 concentration is the lowest near surfaces in the simulation with building geometry and homogenous pollutant emission, which is called the segregation effect. It is concluded that the integrated urban air quality modeling system is a promising modeling approach embracing multiscale influences on urban air quality explicitly.

The urban air quality in the high-rise building area is highly heterogeneous in terms of NO_2 and O_3 concentrations. The building geometry and mobile emission are found to have great impacts on the urban air quality in the CFD simulation. It is likely to be unfeasible to capture the local phenomena in the CMAQ simulation at the corresponding model levels because of low model resolution and insufficient urban surface representation. A mesoscale chemistry-transport model with the assumption of instantaneous well-mixing within a grid cell needs an improvement to consider the spatial variability of urban air quality near the surfaces.

Acknowledgments

The authors are grateful to two anonymous reviewers for providing valuable comments on this work and to Prof. Soontae Kim (Ajou University) for providing the anthropogenic emission inventory (the 2007 CAPSS data) used in the CMAQ model. This work was supported by the National Research Foundation of Korea grant funded by the Korea Ministry of Science, ICT and Future Planning (MSIP) (No. 2011–0017041).

References

Anttila, P., Tuovinen, J.-P., Niemi, J.V., 2011. Primary NO_2 emissions and their role in the development of NO_2 concentrations in a traffic environment. Atmos. Environ. 45, 986–992.
Auger, L., Legras, B., 2007. Chemical segregation by heterogeneous emissions. Atmos. Environ. 41, 2303–2318.
Baik, J.-J., Kang, Y.-S., Kim, J.-J., 2007. Modeling reactive pollutant dispersion in an urban street canyon. Atmos. Environ. 41, 934–949.
Baik, J.-J., Park, S.-B., Kim, J.-J., 2009. Urban flow and dispersion simulation using a CFD model coupled to a mesoscale model. J. Appl. Meteorol. Climatol. 48, 1667–1681.
Beevers, S.D., Kitwiroon, N., Williams, M.L., Carslaw, D.C., 2012. One way coupling of CMAQ and a road source dispersion model for fine scale air pollution predictions. Atmos. Environ. 59, 47–58.
Bright, V.B., Bloss, W.J., Cai, X., 2013. Urban street canyons: coupling dynamics, chemistry and within-canyon chemical processing of emissions. Atmos. Environ. 68, 127–142.
Byun, D., Schere, K.L., 2006. Review of the governing equations, computational algorithms, and other components of the Models-3 Community Multiscale Air Quality (CMAQ) modeling system. Appl. Mech. Rev. 59, 51–77.
Carter, W.P.L., 2000. Documentation of the SAPRC-99 Chemical Mechanism for VOC Reactivity Assessment. Final Report to California Air Resources Board, Contract No. 92–329 and 95–308.
Chen, F., Kusaka, H., Bornstein, R., Ching, J., Grimmond, C.S.B., Grossman-Clarke, S., Loridan, T., Manning, K.W., Martilli, A., Miao, S., Sailor, D., Salamanca, F.P., Taha, H., Tewari, M., Wang, X., Wyszogrodzki, A.A., Zhang, C., 2011. The integrated WRF/urban modelling system: development, evaluation, and applications to urban environmental problems. Int. J. Climatol. 31, 273–288.
Clapp, L.J., Jenkin, M.E., 2001. Analysis of the relationship between ambient levels of O_3, NO_2 and NO as a function of NO_x in the UK. Atmos. Environ. 35, 6391–6405.
Foley, K.M., Roselle, S.J., Appel, K.W., Bhave, P.V., Pleim, J.E., Otte, T.L., Mathur, R., Sarwar, G., Young, J.O., Gilliam, R.C., Nolte, C.G., Kelly, J.T., Gilliland, A.B., Bash, J.O., 2010. Incremental testing of the Community Multiscale Air Quality (CMAQ) modeling system version 4.7. Geosci. Model Dev. 3, 205–226.
Guenther, A., Karl, T., Harley, P., Wiedinmyer, C., Palmer, P.I., Geron, C., 2006. Estimates of global terrestrial isoprene emissions using MEGAN (Model of Emissions of Gases and Aerosols from Nature). Atmos. Chem. Phys. 6, 3181–3210.
Hertel, O., Berkowicz, R., Christensen, J., 1993. Test of two numerical schemes for use in atmospheric transport-chemistry models. Atmos. Environ. 27A, 2591–2611.
Houyoux, M.R., Vukovich, J.M., Coats Jr., C.J., Wheeler, N.J.M., Kasibhatla, P.S., 2000. Emission inventory development and processing for the Seasonal Model for Regional Air Quality (SMRAQ) project. J. Geophys. Res. 105, 9079–9090.
Isakov, V., Touma, J.S., Burke, J., Lobdell, D.T., Palma, T., Rosenbaum, A., Özkaynak, H., 2009. Combining regional- and local-scale air quality models with exposure models for use in environmental health studies. Air Waste Manag. Assoc. 59, 461–472.
Janjić, Z.I., 1994. The step-mountain eta coordinate model: further development of the convection, viscous sublayer, and turbulence closure schemes. Mon. Weather Rev. 122, 927–945.
Jenkin, M.E., 2004. Analysis of sources and partitioning of oxidant in the UK–Part 2: contributions of nitrogen dioxide emissions and background ozone at a kerbside location in London. Atmos. Environ. 38, 5131–5138.
Karim, A.A., Nolan, P.F., 2011. Modelling reacting localized air pollution using computational fluid dynamics (CFD). Atmos. Environ. 45, 889–895.
Kaur, S., Nieuwenhuijsen, M.J., Colvile, R.N., 2005. Pedestrian exposure to air pollution along a major road in Central London, UK. Atmos. Environ. 39, 7307–7320.
Kim, J.-J., Baik, J.-J., 2004. A numerical study of the effects of ambient wind direction on flow and dispersion in urban street canyons using the RNG k–ε turbulence model. Atmos. Environ. 38, 3039–3048.
Kim, M.J., Park, R.J., Kim, J.-J., 2012. Urban air quality modeling with full O_3–NO_x–VOC chemistry: implications for O_3 and PM air quality in a street canyon. Atmos. Environ. 47, 330–340.
Kwak, K.-H., Baik, J.-J., 2012. A CFD modeling study of the impacts of NO_x and VOC emissions on reactive pollutant dispersion in and above a street canyon. Atmos. Environ. 46, 71–80.
Kwak, K.-H., Baik, J.-J., 2014. Diurnal variation of NO_x and ozone exchange between a street canyon and the overlying air. Atmos. Environ. 86, 120–128.
Kwak, K.-H., Baik, J.-J., Lee, K.-Y., 2013. Dispersion and photochemical evolution of reactive pollutants in street canyons. Atmos. Environ. 70, 98–107.
Lee, S.-H., Song, C.-K., Baik, J.-J., Park, S.-U., 2009. Estimation of anthropogenic heat emission in the Gyeong-In region of Korea. Theor. Appl. Climatol. 96, 291–303.
Liu, Y.S., Miao, S.G., Zhang, C.L., Cui, G.X., Zhang, Z.S., 2012. Study on microatmospheric environment by coupling large eddy simulation with mesoscale model. J. Wind Eng. Ind. Aerodyn. 107–108, 106–117.
Matte, T.D., Ross, Z., Kheirbek, I., Eisl, H., Johnson, S., Gorczynski, J.E., Kass, D., Markowitz, S., Pezeshki, G., Clougherty, J.E., 2013. Monitoring intraurban spatial patterns of multiple combustion air pollutants in New York City: design and implementation. J. Expo. Sci. Environ. Epidemiol. 23, 223–231.
Mavroidis, I., Ilia, M., 2012. Trends of NO_x, NO_2 and O_3 concentrations at three different types of air quality monitoring stations in Athens, Greece. Atmos. Environ. 63, 135–147.
Mellor, G.L., Yamada, T., 1982. Development of a turbulence closure model for geophysical fluid problems. Rev. Geophys. Space Phys. 20, 851–875.
Michioka, T., Sato, A., Sada, K., 2013. Large-eddy simulation coupled to mesoscale meteorological model for gas dispersion in an urban district. Atmos. Environ. 75, 153–162.
Moon, N., Kim, S., Byun, D.W., Joe, Y., 2006. Air Quality Modeling System I – Development of Emissions Preparation System with the CAPSS. Korea Environment Institute Report 2006-RE-11.
Ryu, Y.-H., Baik, J.-J., Lee, S.-H., 2011. A new single-layer urban canopy model for use in mesoscale atmospheric models. J. Appl. Meteorol. Climatol. 50, 1773–1794.
Ryu, Y.-H., Baik, J.-J., Kwak, K.-H., Kim, S., Moon, N., 2013. Impacts of urban land-surface forcing on ozone air quality in the Seoul metropolitan area. Atmos. Chem. Phys. 13, 2177–2194.

Shon, Z.-H., Kim, K.-H., Song, S.-K., 2011. Long-term trend in NO_2 and NO_x levels and their emission ratio in relation to road traffic activities in East Asia. Atmos. Environ. 45, 3120–3131.

Skamarock, W.C., Klemp, J.B., Dudhia, J., Gill, D.O., Barker, D.M., Duda, M.G., Huang, X.-Y., Wang, W., Powers, J.G., 2008. A Description of Advanced Research WRF Version 3. NCAR Technical Note NCAR/TN–475+STR.

Stein, A.F., Isakov, V., Godowitch, J., Draxler, R.R., 2007. A hybrid modeling approach to resolve pollutant concentrations in an urban area. Atmos. Environ. 41, 9410–9426.

Tewari, M., Kusaka, H., Chen, F., Coirier, W.J., Kim, S., Wyszogrodzki, A.A., Warner, T.T., 2010. Impact of coupling a microscale computational fluid dynamics model with a mesoscale model on urban scale contaminant transport and dispersion. Atmos. Res. 96, 656–664.

Vardoulakis, S., Solazzo, E., Lumbreras, J., 2011. Intra-urban and street scale variability of BTEX, NO_2 and O_3 in Birmingham, UK: implications for exposure assessment. Atmos. Environ. 45, 5069–5078.

Wang, Y.J., DenBleyker, A., McDonald-Buller, E., Allen, D., Zhang, K.M., 2011. Modeling the chemical evolution of nitrogen oxides near roadways. Atmos. Environ. 45, 43–52.

Wyszogrodzki, A.A., Miao, S., Chen, F., 2012. Evaluation of the coupling between mesoscale-WRF and LES-EULAG models for simulating fine-scale urban dispersion. Atmos. Res. 118, 324–345.

Zhong, J., Cai, X.-M., Bloss, W.J., 2014. Modelling segregation effects of heterogeneous emissions on ozone levels in idealised urban street canyons: using photochemical box models. Environ. Pollut. 188, 132–143.